Engineering Failure Analysis 174 (2025) 109460

Contents lists available at ScienceDirect

Engineering Failure Analysis

journal homepage: www.elsevier.com/locate/engfailanal

Effect of bio-mimicked surface texturing on the shear strength of additively manufactured metal single-lap joints: An innovative approach

M. Gokhan Atahan [a,b,*], Ian Maskery [a], Ian Ashcroft [a], M. Kemal Apalak [c], Athanasios Pappas [d]

[a] Centre for Additive Manufacturing, University of Nottingham, Nottingham NG8 1BB, UK
[b] Department of Mechanical Engineering, Abdullah Gul University, Kayseri 38080, Turkiye
[c] Department of Mechanical Engineering, Erciyes University, Kayseri 38030, Turkiye
[d] Manufacturing Metrology Team, University of Nottingham, Nottingham NG8 1BB, UK

ARTICLE INFO

Keywords:
Bio-mimicking
Additive manufacturing
Mechanical interlocking
Adhesive joint
Wettability
Shear test

ABSTRACT

In this paper, we investigate the mechanical performance of metal single-lap joints featuring bio-mimicking surface textures. The inspiration for the surface textures was the foot and toe of the gecko, a creature whose ability to climb smooth shear surfaces is attributed to the meso- and micro-structures of its feet. Three surface textures were investigated: a hexagonal texture based on the central region of the foot, a lamellae-like texture based on the toe, and a mixed texture of both. Metal adherends with these textures were produced using the laser powder bed fusion (LPBF) additive manufacturing method. Finite element analysis was performed to examine the influence of surface texture on stress distribution in the adhesive layer, while mechanical testing was used to determine joint strength and failure mode. Compared to the as-printed surface texture, bio-mimicking surface textures improved the wettability of the bonding surfaces, and significantly improved the lap shear strength of the joints. Mechanical interlocking due to surface texture was more effective than the increase in bonding surface area in enhancing joint strength. The bio-mimicking textures improved the damage tolerance capacity of the joints by reducing local stress concentrations at the overlap edges of the adhesive layer and ensured that the adhesive failure type was mixed mode due to the mechanical interlocking effect. The presented novel bio-mimicked surface texture method offers promising results for both industrial applications and scientific studies.

1. Introduction

Adhesive joints are widely used in automotive, aerospace, and marine industrial sectors due to their ability to join dissimilar materials. The mechanical properties of these joints depend on adhesive and adherend properties, surface treatment, and joint geometry [1–3]. Various methods, including laser surface texturing, electro-discharge and electrochemical machining, cutting, lithography, and micro-forming processes, have been used to add surface texture to adhesive joint interfaces, with the aim of enhancing their strength [4]. Laser surface texturing enables the production of complex and hierarchical surface textures, but the associated high-energy pulses can cause deterioration of the surfaces through repeated thermal cycling [4].

* Corresponding author at: Department of Mechanical Engineering, Abdullah Gul University, Kayseri 38080, Turkiye.
E-mail address: mithatgokhan.atahan@agu.edu.tr (M.G. Atahan).

https://doi.org/10.1016/j.engfailanal.2025.109460
Received 10 January 2025; Received in revised form 11 February 2025; Accepted 24 February 2025
Available online 3 March 2025

The production of adherends and surface texturing can be performed simultaneously with additive manufacturing (AM), providing a time saving over multi-step production processes. Several researchers have examined the use of AM for textured joint production [5–8]. Of those AM processes available for the production of metal parts, laser powder bed fusion (LPBF), based on building a 3D part through the successive remelting of powders in layers, is the most widely used. Surface textures for adhesive joints can be categorized into four groups; stochastic, isotropic, anisotropic, and structural surfaces [4,9]. Recently, researchers have focused on functionally structured surface textures to increase joint strength rather than stochastic surfaces [10–24]. The aim of controlling the surface texture design parameters is that poor wettability caused by excessive surface roughness is prevented, the desired joint strength is achieved and directional joint strength can be engineered if desired.

Nature provides us with excellent design examples for surfaces. Bio-inspired surfaces can provide super hydrophilic surface properties, allowing an adhesive to spread effectively on the bonding surface and significantly increase the joint strength [4,25,26]. Numerous researchers have examined the effect of bio-inspired surface textures on the mechanical behaviour of adhesive joints. Alfano et al. [27] investigated the fracture behaviour of bio-inspired interfaces with a double cantilever beam test. They determined that the bio-inspired interface caused a significant increase in the total dissipated energy compared to the specimens with no surface texture. Wan et al. [28] enhanced the wettability and bonding strength of aluminium joints with the bio-inspired surface texture. Naat et al. [25] developed new surface textures inspired by fish scales and tree frog toe pads for adhesive joints. The developed bio-inspired surface textures were produced by additive manufacturing. They reported that fish scale and tree frog toe pad-inspired surface textures increased the shear strength considerably. In further work, Naat et al. [26] found that the highest increase in joint strength was achieved in the tree frog hierarchical hexagonal texture, while the lowest shear strength occurred when the printed surface was abraded with P1000 grit paper. Bu et al. [29] increased the shear strength and toughness of carbon fibre-reinforced composite-metal joints with fishbone and nacre-inspired surface textures. However, studies of directly bio-inspired surface texture are still very limited in the literature, with surface textures prepared considering the geometric shapes of inspired structure being used rather than the true surfaces seen in nature. A common simplification is to use repetitive geometric structures in generating the surface textures. However, structures in nature often have a range of unit cells with different geometric properties [30]. Therefore, truly bio-inspired surfaces should be based on measurements of natural surfaces rather than the use of duplicating unit cells with similar geometry. The high surface adhesion of a gecko's foot surface is derived from its hierarchical surface structure and super hydrophilic surface condition. Since the gecko's foot surface structure is expected to increase the strength of adhesive joints, the gecko's foot and toe surface structure were considered in this research [25].

In this study, the mechanical performances of adhesive joints with gecko toe and foot surface textures were investigated experimentally and numerically. Three different surface textures were considered; those based on the gecko's toe, the foot, and a combination of both. Metal adherends with the desired surface texture were manufactured in a single step by LPBF from 316 L stainless steel powder. The surface textures were generated using a photographic image of a gecko. The effects of the bio-mimicking surface texture on the shear strength of the joint were investigated and compared with joints having no surface texture (referred to as an "as-printed" surface structure). Finite element analysis was carried out to determine the effect of the true surface texture on the stress distribution on the adhesive surfaces, enabling correlation with the observed failure modes of the physically tested specimens.

2. Experimental study

2.1. Design

In this study, three different surface textures were designed considering the gecko's foot and toe surface textures. The true surface textures were created on the adherend bonding surfaces. The imitating surface texture process of the adhesive joint is shown in Fig. 1. Gecko's foot and toe surface photos with a square shape were generated from photographic images of a gecko's photo from the U.S. National Science Foundation website with usage permission [31], as shown in (Fig. 1a). The overlap region of the adhesive joint is square with 25 × 25 mm dimensions. The gecko's surface photographs were obtained with a square geometry and thus the true geometric ratio of the surface texture was preserved. Adherends with the different surface textures were designed using Solidworks software [32], and true surface textures were created with the 3D Texture command (Fig. 1b,c). The maximum surface texture depth was chosen as 0.8 mm and the surface texture depth was automatically adjusted by the software according to the grey scale. As a result, surface textures with varying depths ranging from 0 to 0.8 mm were obtained. To avoid adhesive penetration problems, the maximum surface texture depth was set to less than 1 mm [4,26]. The created surface textures are presented in Fig. 2. It can be seen that the texture from the palm of the foot has a hexagonal structure whilst that from the toes is striated, hence, in this work we refer to these textures as hexagon-like and lamellae-like. Three different types of surface textures were created based on the Gecko's inner foot surface, the toe, and a combination of both. Single-lap joints were manufactured according to the ASTM D1002-10 test standard [33], with dimensions as shown in Fig. 3. The overlap length of 25 mm is within the limit allowed by the test standard. In order to preserve the geometric ratio of the surface textures, a square overlap region is required.

2.2. Specimen manufacturing

STL files of the designed adherends were created with Materialise Magics software [35]. Then, manufacturing codes were generated with Renishaw QuantAM software [36]. The adherends were manufactured from 316 L stainless steel powder using a Renishaw AM 125 Laser Powder Bed Fusion (LPBF) machine (Fig. 4a). Printing parameters are shown in Table 1. The scan strategy

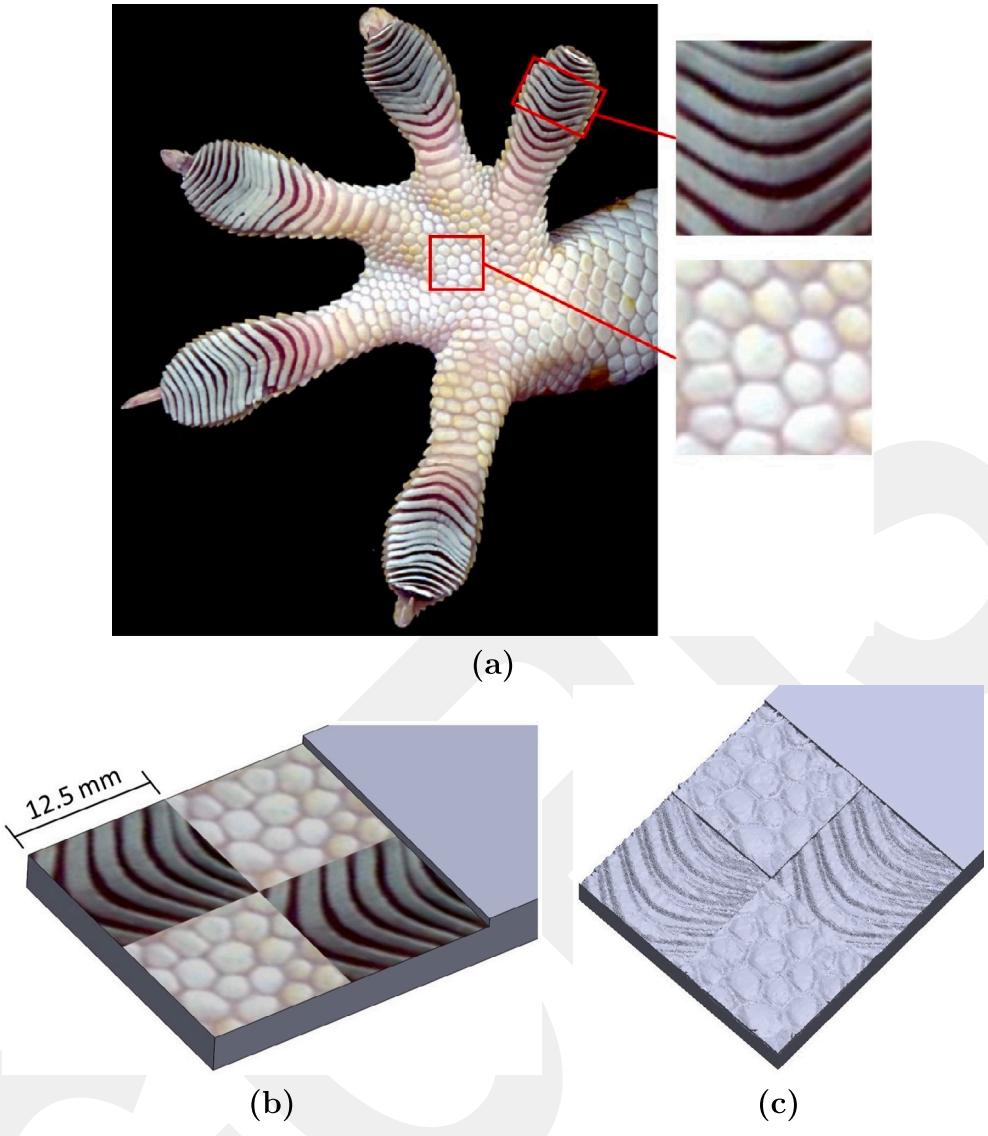

Fig. 1. (a) Surface textures from photographic image of a gecko's toe and foot [31,34], (b) placement of surface images on the overlap region of an adherend, (c) creating surface textures with the 3D Texture command.

was a meandering pattern with a rotation angle of 67 degrees. The build plate was heated to 80 °C throughout processing. An argon atmosphere was used to keep the oxygen content below 500 ppm during fabrication. The particle size distribution was 15-45 μm, as determined by laser diffraction. The 316 L stainless steel powder was purchased from Carpenter Technology and the mechanical properties from standard tensile test specimens manufactured from this powder by LPBF are presented in Table 2. Araldite Standard [37], a two-component epoxy adhesive, was used as the adhesive for bonding printed adherends. The elastic modulus and Poisson's ratio of Araldite Standard adhesive were found to be 930 MPa and 0.32, respectively [38]. Adherend bonding surface cleaning ensures a good bonding strength for single-lap joints. In order to remove dirt, remaining powder, and other residues on the bonding region, the adherend bonding surfaces were cleaned with isopropanol before applying the adhesive. The adhesive was applied evenly to the adherend surface (Fig. 4b) and clamping clips were used to apply pressure whilst curing (Fig. 4c). The excess adhesive was removed from the edges of the joint before curing at room temperature for 48 h.

2.3. Surface characterization

Surface characterization consisted of: measurement of the topography, evaluation of the wettability, and observation of penetration between the adherends and the adhesive. The surface topography measurements were performed using a Sensofar Sneox 3D profiler, which is an optical instrument fitted with three different measurement modes, namely coherence scanning

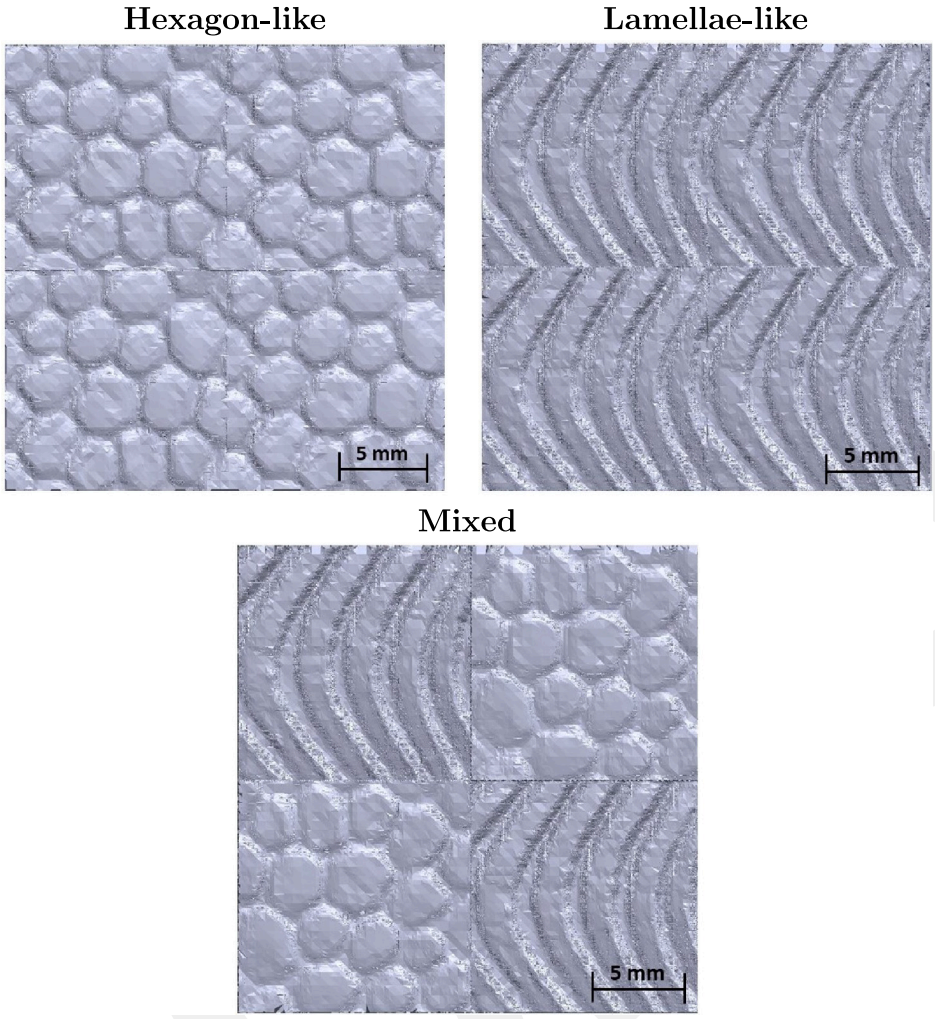

Fig. 2. Demonstration of the bio-mimicked surface texture designs.

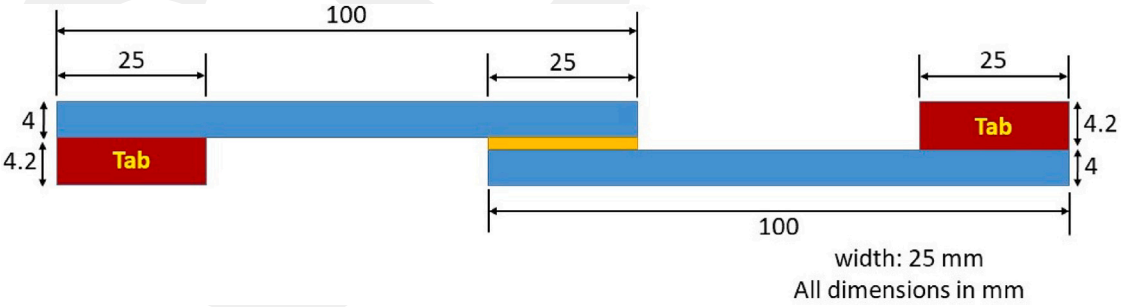

Fig. 3. Dimensions of the single-lap joint.

interferometry, confocal microscopy (CM), and focus variation (FV) microscopy. FV was the preferred mode of measurement due to it being a more time-efficient measurement process and, as the reconstruction algorithm of the FV mode is based on the contrast present in the bright-field image, it achieves better results in comparison to the other modes. An overview of the specifications of the bright-field objective used for the measurements is presented in Table 3. After the measurements were completed the measured topographies and their corresponding reference data (STL file) were compared using Mountains Map [40]. As the reference measurements were generated using design software, they had to be converted to facilitate the comparison. Thus, the triangular

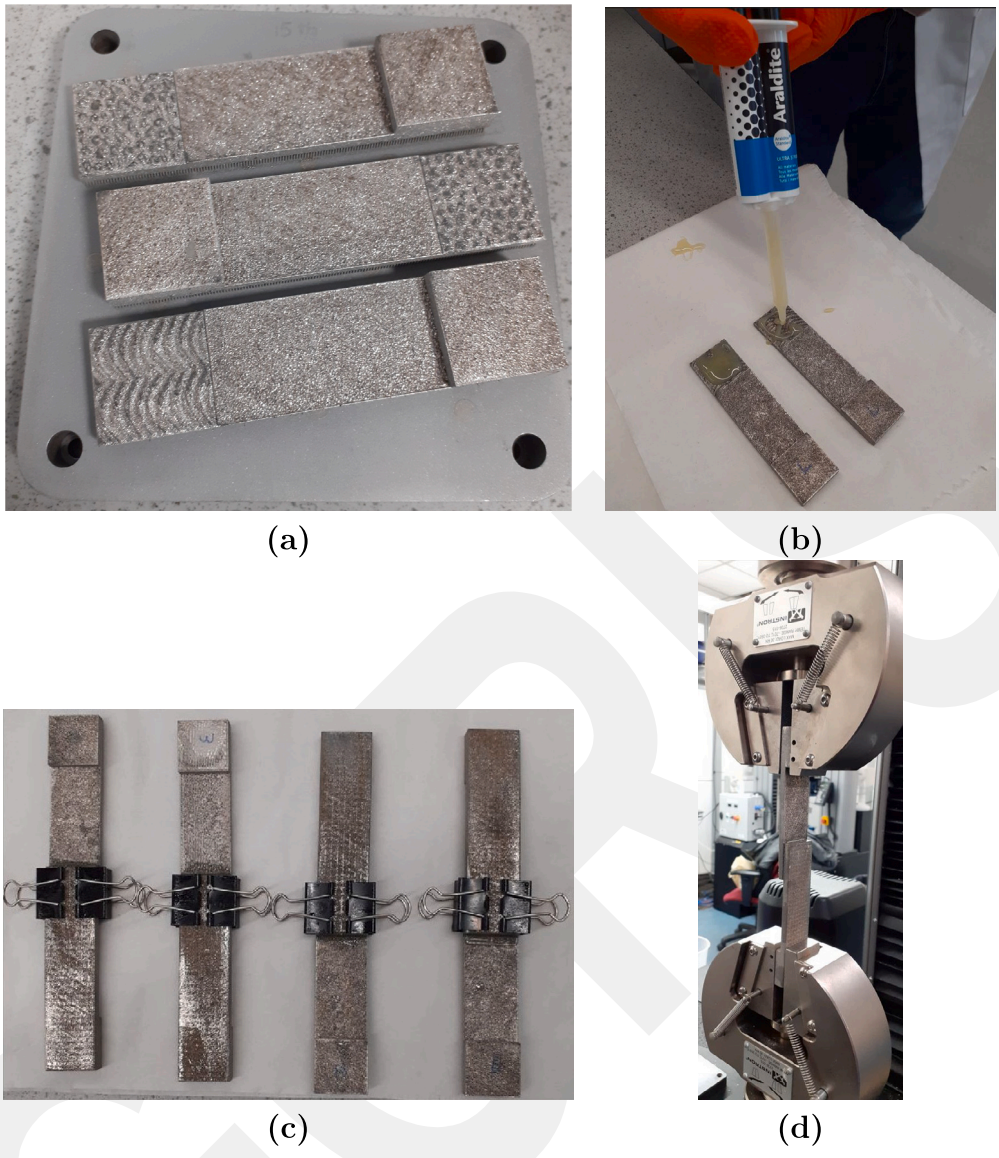

Fig. 4. (a) Printed adherends with bio-mimicked surface textures, (b) applying adhesive to the adherend's surface, (c) curing the lap joints, (d) tensile shear testing.

Table 1
Metal printing process parameters.

Laser power	160 W
Powder material	316 L stainless steel
Exposure time	50 μs
Layer thickness	30 μm
Hatch distance	50 μm
Spot size	44 μm
Scan speed	0.72 m/s

Table 2
Mechanical properties of printed 316 L stainless steel [39].

Elastic modulus	Yield strength	Ultimate tensile strength	Elongation at break
179 GPa	485 MPa	585 MPa	55%

Table 3
Objective specifications for the FV mode of the measuring instrument.

20x bright-field objective specifications	
Numerical aperture (NA)	0.55
Optical resolution	0.52 μm
Field of view (FOV)	0.17 mm
Spatial sampling	0.17 μm

mesh of the measurements was converted into an x-y matrix of height coordinates using Mountains Map. The application of the algorithm is based on matching specific pixels between the reference and the measured data to ensure comparison of the same area. Hence, the application of the algorithm shifts the matrix of the measured data both in translation and rotation in order to match to the reference one. Finally, bandwidth matching was performed using Gaussian convolution S- and L- filters. The measured surfaces were evaluated using a commercial surface topography measuring instrument equipped with confocal technology. The objective lens used was a 20× magnification objective with a 0.34 μm spatial sampling distance. Following the ISO 25178 Part 3 Specifications [41], an S nesting index (S-filter) of 0.002 mm was chosen. Then, considering a bandwidth ratio of 1:100 an L-nesting index of 0.2 mm was chosen to separate the roughness from the waviness component of the primary surface and obtain the roughness parameters. Since repetitive surface textures were used in the overlap region, surface topography measurements were carried out by considering an area of 12.5 × 12.5 mm covering a single surface texture. The designed surface in the STL file and the produced surfaces were compared to assess the ability of LPBF to generate the desired textures.

Static contact angle measurement provides information about the wettability of the adherends. The static contact angle of the bio-mimicked surface textures was measured using the sessile drop method using a KRUSS DSA 100 device [42]. The contact angle measurements were performed under atmospheric conditions using a 5 μL volume of distilled water. The 5 μL volume of distilled water was dropped on the overlap region and a droplet contact photograph was taken after stabilization to determine the water contact angle (WCA) measurement. However, the bio-mimicked surfaces showed super-wetting behaviour with the dropped water being completely dispersed on the surface at equilibrium. For this reason, each contact angle measurement was recorded on video, and the spreading stages of the droplet were obtained as photographs from this video [26]. Each video was converted into a 20-frame photo reel. Since bio-mimicked surfaces have highly anisotropic properties, contact angle measurements were repeated many times with different surface locations.

In order to obtain high-strength joints, the applied adhesive must penetrate well into the adherend bonding surface. To observe the penetration of the adhesive into the bio-mimicked bonding surfaces, cross-sections of the adhesive joint with the mixed type surface texture were polished and cross-sectional images of the joint area examined to observe the degree of penetration.

2.4. Lap shear test

The lap shear tests of the adhesively bonded single-lap joints were carried out according to ASTM D1002-10 [33]. An Instron tensile test machine [43] with a 30 kN load cell was used for the lap shear tests, as shown in Fig. 4d. The lap shear tests were performed at room temperature with a cross-head speed of 1 mm/min. Three repeated tests were conducted for each surface texture design to validate the experimental results. Force and displacement values were recorded during the test. The lap shear strength of the bonded joints was determined by dividing the maximum load by the overlap area. The failure mechanism of the joints was observed optically. In this way, the effect of the surface textures on the adhesive failure mechanism was determined.

3. Finite element model

In order to better understand the experimental results, the effects of surface texture on stress distribution in the adhesive layer were analysed by three-dimensional finite element analyses of the single-lap joints using ABAQUS [44]. Surface textures can potentially increase the strength of an adhesive joint by providing additional mechanical interlocking between the adherend and the adhesive. An insight into the effect of a surface texture on the performance of the joint can be investigated by determining the effect of the surface texture on the stress distribution in the adhesive. In the transformation of surface textures into the finite element model, the adherend with a surface texture was exported in STL file format using Solidworks software. The STL file of the adherend was imported into the numerical model and converted to a solid using a plug-in. Surface textures were then subtracted from the adhesive surfaces with the Merge/Cut instances command in the assembly module. In this way, the contact penetration of the adhesive inside the adherend surface texture was created and the potential mechanical interlocking between the adhesive and the adherend could be predicted. The surface textures created on the adhesive surface and the finite element model of the single-lap joint are shown in Fig. 5. Adherend and adhesive interfaces were combined with the Tie command. An elastic material model was used for adherend and adhesive as the aim of this exercise was to investigate the stress distribution under load rather than to directly predict failure. A reference point at the end of each adherend was added to define constraints and loading conditions. While one of the adherend's motions was prevented in any coordinate direction, a displacement of 0.035 mm was applied along the x-axis for the other adherend. Adherends and adhesive were modelled using three-dimensional quadratic tetrahedral elements (C3D10). To determine the effect of mesh size on the numerical result, four different element length sizes, 1, 1.5, 2, and 2.5 mm, were tested for the joint with the as-printed surface. The change in results from 2.5 mm to 1 mm was less than 1%. Therefore, the results were not

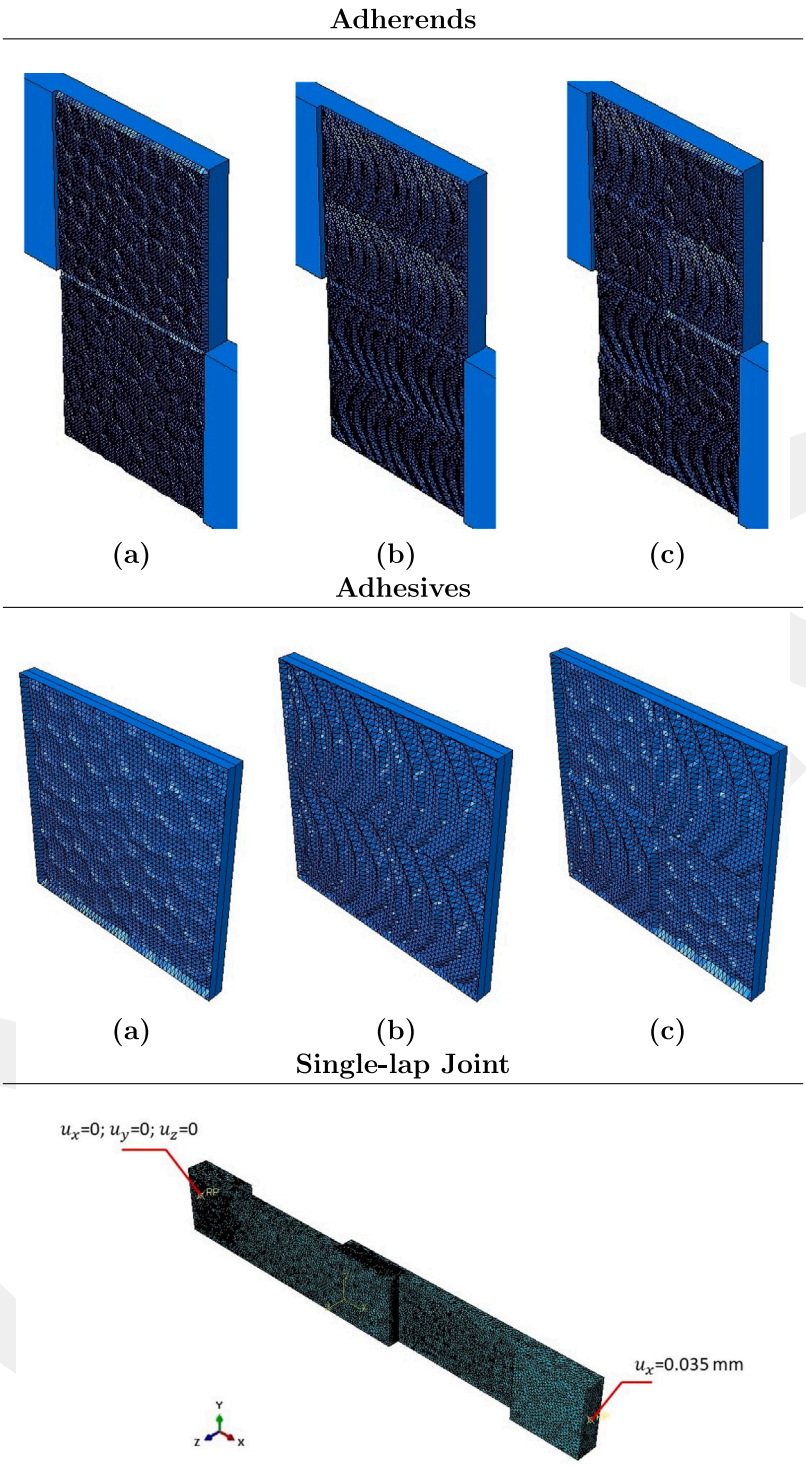

Fig. 5. Demonstration of the adherends and adhesive surfaces (a: hexagon-like, b: lamellae-like, and c: mixed) and numerical model of the single-lap joint (u_x: axial displacement in x direction).

significantly affected by the mesh size. The mesh element size of the adherend and adhesive was set to 1 mm for all joints. Since plastic deformation has not yet occurred in the adhesive at a displacement of 0.035 mm (as the experimental force–displacement curve shows a linear variation), using the elastic material model for the adhesive is sufficient to obtain accurate result. The numerical

Table 4
Surface height parameters of designed and manufactured surfaces.

	S_a (μm)	S_q (μm)	S_p (μm)	S_v (μm)	S_z (μm)
As-printed	52.19	67	341.20	194.30	535.50
Hexagon-like (Designed)	169.70	198.50	308.70	491.30	800
Hexagon-like (Manufactured)	83.10	104.10	384.00	413.30	797.30
Lamellea-like (Designed)	192.70	222.20	399.40	400.60	800
Lamellea-like (Manufactured)	93.73	117.60	393.80	403.40	797.30

results were validated by comparing the experimental and numerical force values corresponding to a displacement of 0.035 mm for the joints with each surface texture design. Since the difference between the experimental and numerical force values varies between 10%–20%, it was determined that the developed numerical model provides realistic and reliable results.

4. Results and discussion

4.1. The effect of the surface textures on the surface morphology

The designed and manufactured surface morphologies in the overlap region of the adherends are compared in Fig. 6. The design for the "as-printed" joint was nominally flat and smooth, however, it can be seen that there is residual melted metal powder on the surface of the overlap region, which is a characteristic of LPBF. These powders create a natural surface texture on the surface. Hence, the joint without an engineered surface texture is called "as-printed" in this study. It can be seen that this powder created surface can be seen superimposed on the engineered hexagon-like and lamellae-like surfaces in Fig. 6.

Both engineered surface textures have depths varying between 0–0.8 mm in both the design and the manufactured specimen. It was observed that hexagon-like and lamellae-like surface textures are produced successfully in accordance with the designed dimensions and shapes using the LPBF additive manufacturing method. While the depth of the hexagon-like surface texture ranges from 0.25 to 0.8 mm, the depth of the lamellae-like surface texture ranges from 0.1 to 0.8 mm. Therefore, the lamellae-like surface texture may allow the adhesive to penetrate more deeply, thereby providing better mechanical interlocking. However, compared to the hexagon-like surface texture, the lamellae-like surface texture has sharper geometries, which may cause local stress concentrations and negatively affect the joint strength.

Table 4 shows the surface height parameters of the designed and manufactured surfaces. Two commonly used parameters for characterizing the surface textures are S_a and S_q. S_a refers to the arithmetical mean deviation of the assessed surface while S_q is the root mean square deviation of the assessed surface. These parameters are lowest for the as-printed surface and largest for the Lamellea-like surface. The other three parameters of interest are S_p, S_v, and S_z with S_p denoting the maximum peak height of the surface from the mean plane, S_v the maximum valley depth of the surface, and S_z a sum of the maximum peak and valley of the surface. Since the depth values of hexagon-like and lamellae-like surface textures were adjusted with a similar approach, these surface parameters were close to each other.

As seen in Table 4, the desired maximum depth values (S_z) of the designed surface textures are 800 μm. The S_z values of the manufactured Hexagon-like and Lamellea-like surface textures were measured as 797.30 μm. Therefore, it was determined that the designed and manufactured surface textures had similar maximum depth values and the LPBF additive manufacturing method was successful in producing complex surface textures. Although there was no designed surface texture on the as-printed surface, the powders created a natural surface texture due to the characteristic powder used in LPBF and the S_z value of this surface was determined as 535.50 μm.

The wettability of the different manufactured surfaces was evaluated by contact angle measurement. A surface with a water contact angle (WCA) value greater than 90° is termed hydrophobic as water droplets do not spread on the surface, while a surface with a WCA less than 90° is hydrophilic as water spreads homogeneously on the surface [45–47]. The average static contact angle values and representative spreading stages of the droplet of bio-mimicked and as-printed surfaces are shown in Fig. 7. Since the average WCA was 48°, the as-printed adherend surface showed hydrophilic behaviour. However, as seen in Fig. 7, the water droplets on the bio-mimicked surfaces spread completely, i.e. WCA = 0°. This shows that the bio-mimicked surfaces have super-hydrophilic characteristics, that is they have super-wetting behaviour. A similar observation was reported by Naat et al. [26].

Cross-sectional views of the joint with a mixed surface texture are presented in Fig. 8a. After the adherends with a mixed surface texture were produced using the LPBF process, the bonding surfaces were cleaned with isopropanol and then bonded using an epoxy-based adhesive. After the single-lap joint was cured, it was precisely cut from the overlap region using a precise cutting machine. Finally, the cutting surface was polished, and cross-sectional views were obtained. Since the joint with the mixed surface texture contains both engineered surfaces (hexagon-like and lamellae-like), it provides the opportunity to observe the penetration of the adhesive in both surface textures. It was observed that the adhesive had good penetration into both surface textures, thus providing mechanical interlocking between the adhesive and the adherend. The super-hydrophilic behaviour of the bonding surface plays an important role in the penetration of the adhesive into the surface textures. The air trapped at the interface between the adherend and the adhesive can be easily evacuated and strong capillary forces drive the adhesive into the surface textures [26]. Fig. 8b shows an SEM (Scanning Electron Microscope) image of the bonding region with a mixed surface texture. An SEM image of the metal adherend sample was captured without sputter coating. The acceleration voltage was 15 kV. Since a detailed surface

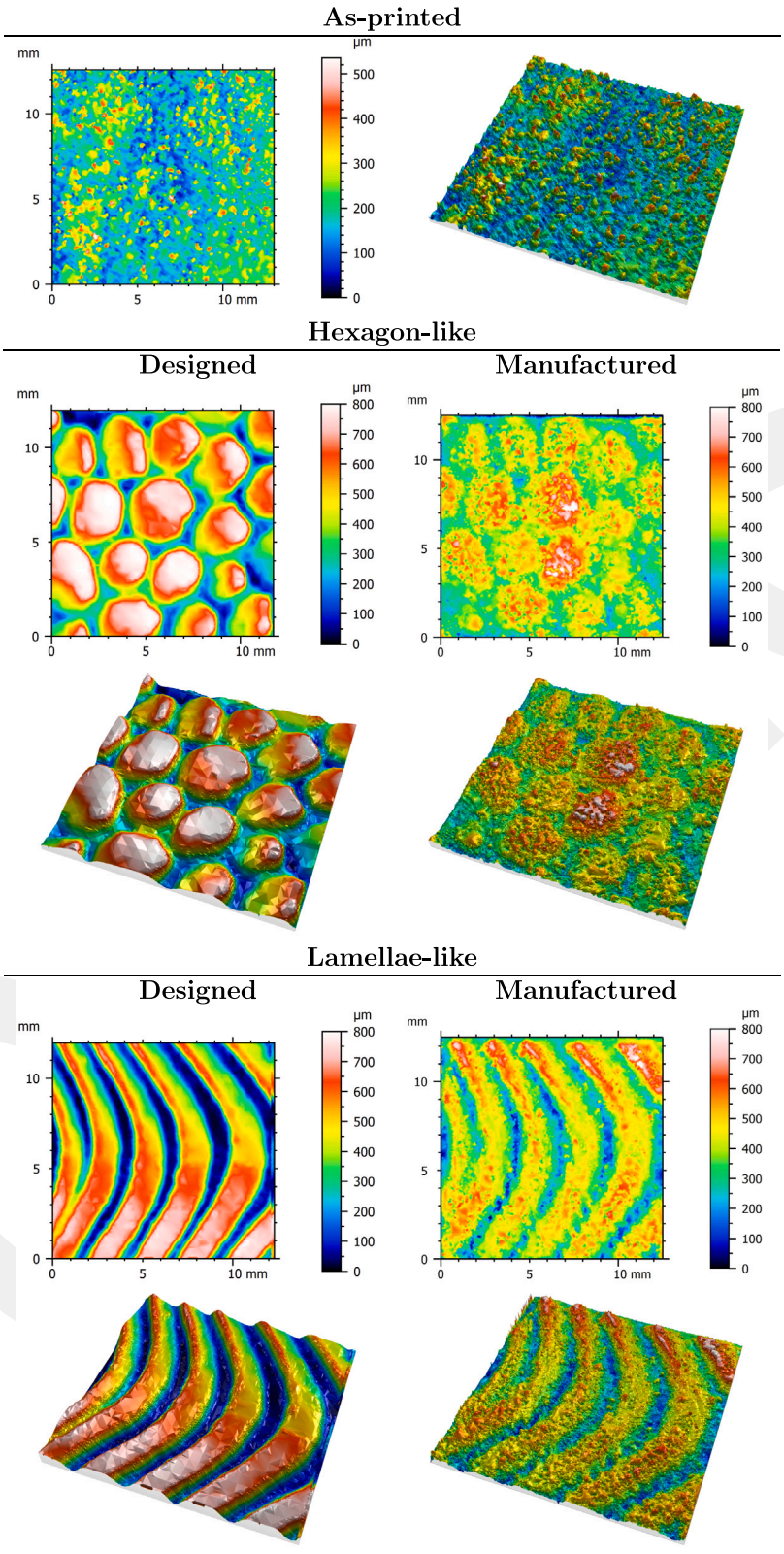

Fig. 6. Comparison of the designed and manufactured surface topography maps.

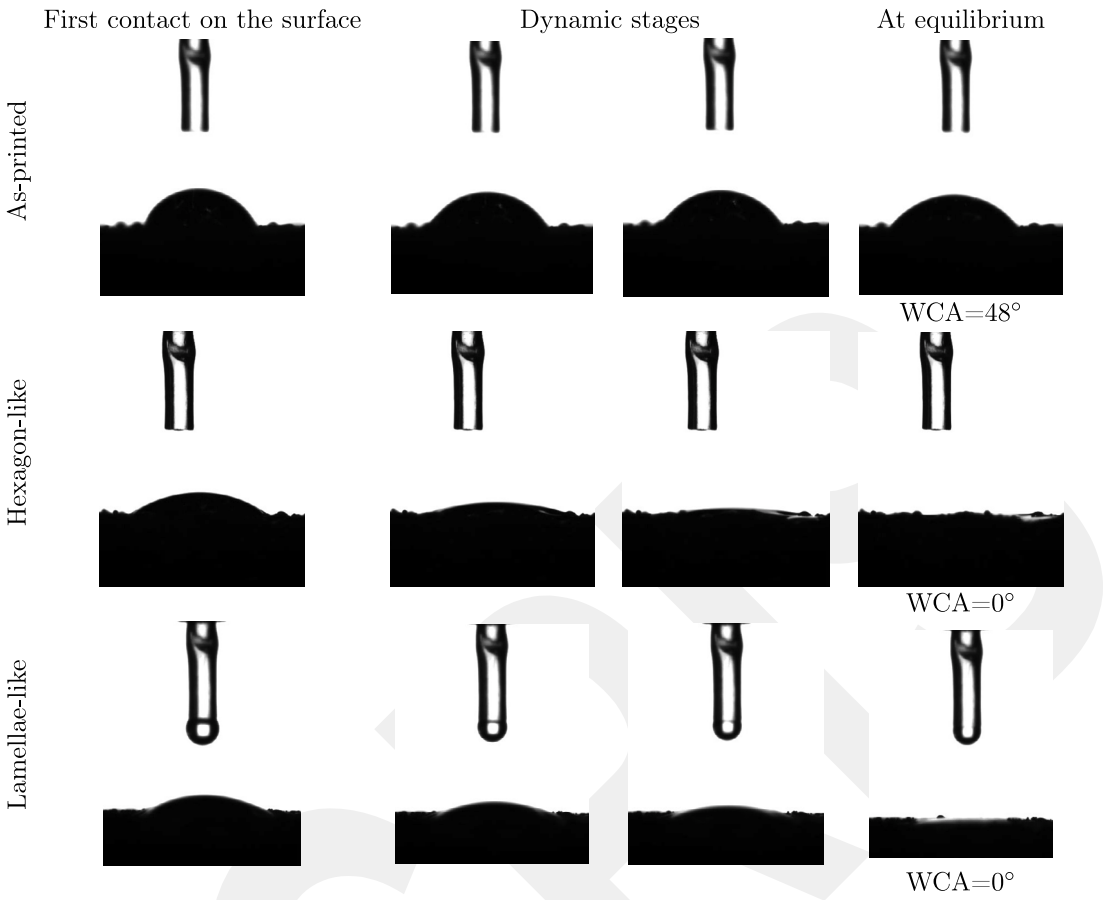

Fig. 7. The spreading stages of the droplet on the printed surfaces.

analysis was not required in this study, the obtained SEM image was deemed sufficient to observe production defects. Small pores and irregular melted parts were observed on the manufactured surfaces. Pores and irregular melting occur due to the effect of trapped gases, and a lack of fusion [26,48]. Since the LPBF additive manufacturing method is based on the principle of melting metal powders, partially melted powders were observed on the manufactured surfaces.

4.2. The effect of the surface textures on the lap shear strength

In this section, the effect of bio-mimicked surface textures on the failure load and lap shear strength of the additively manufactured adhesive joints is examined. Representative force–displacement plots from the lap shear tests are shown in Fig. 9. Additionally, the average failure load values of the adhesively bonded joints are presented in Table 5. The average failure load values for as-printed, hexagon-like, lamellae-like, and mixed surface textures are 4.84 kN, 8.47 kN, 6.61 kN, and 10.59 kN, respectively. It is significant that the bio-mimicked surface textures resulted in considerable increases in the load-carrying capacity of the joints compared to the as-printed surface. The force–displacement plots show a similar slope for all joints in the elastic deformation region, as expected as this is determined primarily by the elastic properties of adhesive and adherend. However, the failure load and extension at failure increase significantly with the engineered surfaces, with the mixed surface texture showing more than double the failure load and almost treble the extension at failure.

The nominal and real lap shear strength values of adhesive joints are shown in Table 6. The nominal lap shear strength of adhesive joints was obtained by dividing the average failure load by the area of the overlap region assuming a flat surface (625 mm^2). The calculated surface areas of the different surface textures were determined using STL files, and the percentage increase in bonding area was calculated relative to the flat surface area (Table 5). Nominal lap shear strength was based on assuming a flat surface, while the real lap shear strength was determined according to the calculated surface area. The as-printed surface was used as a reference to evaluate the effect of bio-mimicked surface textures on the increase in lap shear strength. Compared to the as-printed surface, the lamellae-like surface texture resulted in a 23.94% (real) - 36.57% (nominal) increase in lap shear strength, while the hexagon-like surface texture led to a 63.61% (real) - 75% (nominal) increase. Although the lamellae-like surface texture resulted in the greater increase in bonding surface area, the hexagon-like surface texture provided a greater increase in lap shear

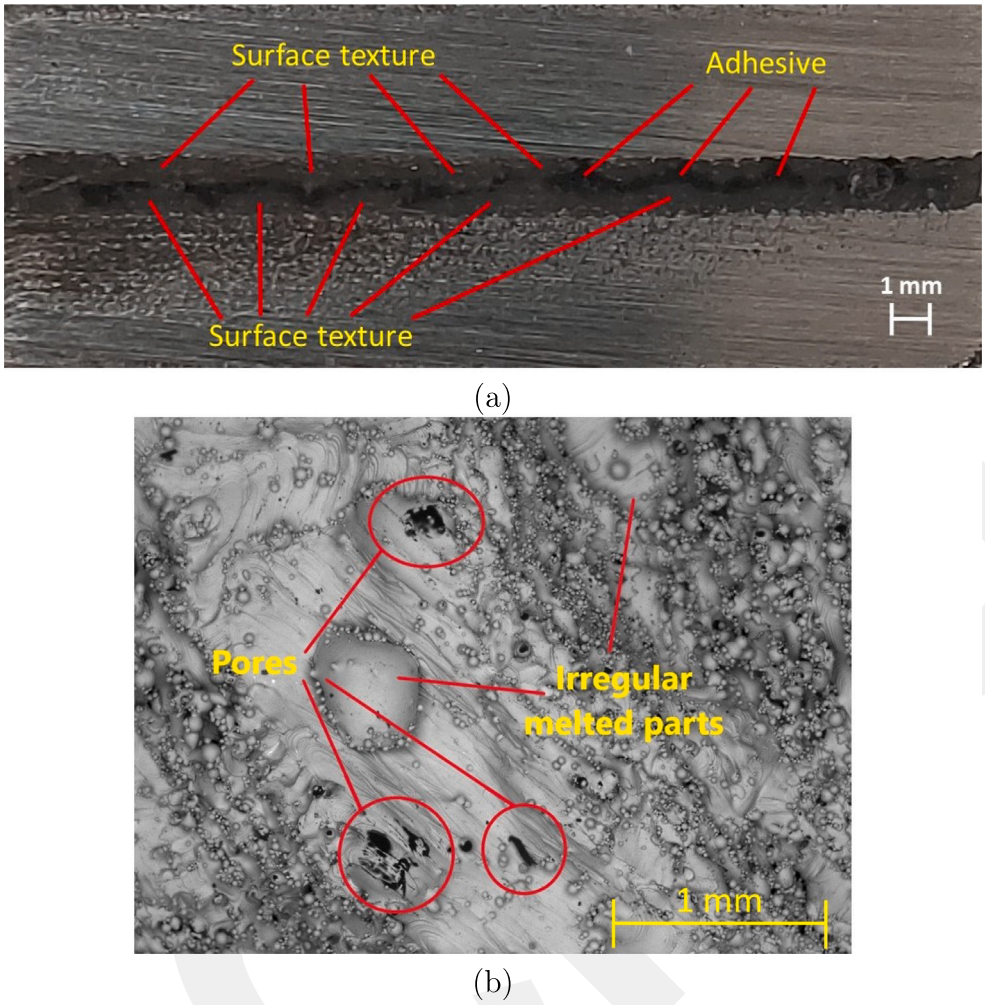

Fig. 8. Cross-sectional image of the adhesive joint with a mixed surface texture.

Table 5
The nominal and calculated bonding surface areas and average failure load values of adhesive joints.

Surface type	Nominal surface area (mm^2)	Calculated surface area (mm^2)	Increase in bonding area (%)	Average failure load (kN)
As-printed	625	625	–	4.84 ± 0.06
Hexagon-like	625	668.53	6.96	8.47 ± 0.14
Lamellae-like	625	688.71	10.19	6.61 ± 0.62
Mixed	625	684.81	9.57	10.59 ± 1.41

strength. This result showed that the surface texture geometry was more effective in increasing the adhesive joint strength than the increase in surface area. While the largest increase (99.69% (real) - 118.80% (nominal)) in shear strength was observed in the joint with the mixed surface texture, the smallest increase (23.94% (real) - 36.57% (nominal)) occurred in the joint with the lamellae-like surface texture. For the joint with the mixed surface texture, dissimilar surface textures coincided with one another. Therefore, the mechanical interlocking effect of both hexagon-like and lamellae-like textures played an important role together, resulting in the highest shear strength. Two main factors affect the lap shear strength when surface textures are used in adhesive joints. That is, the surface texture increases the effective bonding surface area to withstand shear load and the surface texture geometry provides the mechanical interlocking to improve joint strength [4,26]. In this study, it was found that mechanical interlocking due to surface texture was more effective than the increase in bonding surface area in improving joint strength. Furthermore, the bio-mimicked surface textures significantly improved the lap shear strength of the adhesive joint by providing mechanical interlocking, thanks to their unique, complex geometry.

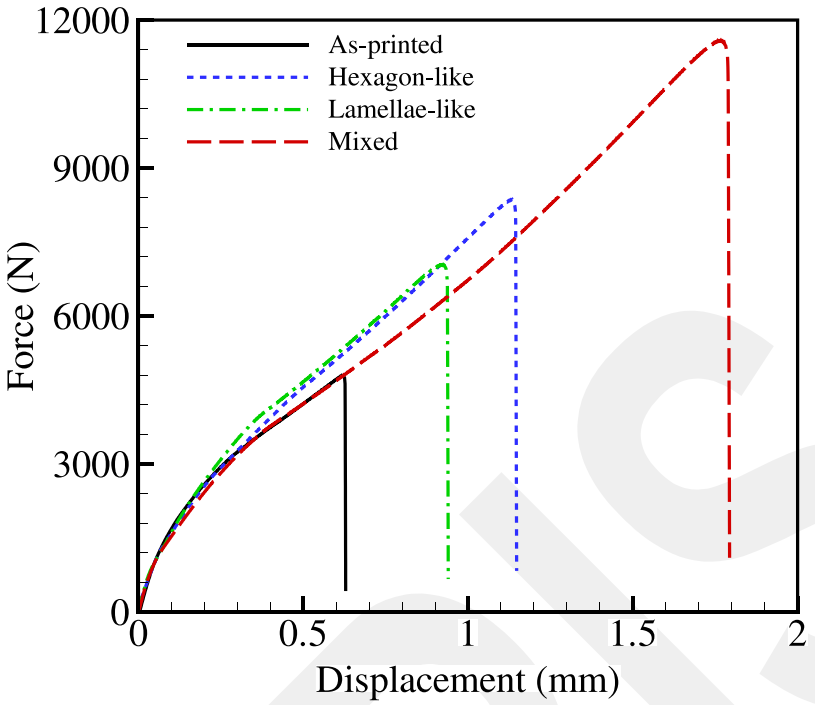

Fig. 9. Representative force–displacement curves of the single-lap joints with different surface textures.

Table 6
Shear strength values of adhesive joints.

Surface type	Average nominal lap shear strength (MPa)	Increase in nominal shear strength (%)	Average real lap shear strength (MPa)	Increase in real shear strength (%)
As-printed	7.74 ± 0.09	–	7.74 ± 0.09	–
Hexagon-like	13.55 ± 0.23	75	12.67 ± 0.22	63.61
Lamellae-like	10.58 ± 0.99	36.57	9.60 ± 0.90	23.94
Mixed	16.94 ± 2.25	118.80	15.46 ± 2.06	99.69

4.3. The effect of the surface textures on the stress distribution

The effect of the bio-mimicked surface texture on the stress distribution of the adhesive layer was examined by 3-D finite element analysis. The mechanical performance of adhesive joints can be evaluated by considering shear, peel, and von Mises stress distributions. Adhesive joints are often subjected to shear loads in industrial applications. Therefore, the effect of the surface texture on the shear stress distribution of the adhesive layer is important to evaluate joint performance. Load eccentricity occurs in the single-lap joint geometry under tensile load. This eccentricity causes a bending moment in the overlap region which generates a peel stress, which increases at the edges of the overlap area. This tensile stress can be critical in initiating failure in the single lap joint. The von Mises stress is a combined stress state and is associated with determining the damage tolerance of adhesive joints.

The shear stress distributions of the adhesive surfaces are presented in Fig. 10. In the finite element analysis, the designed texture free (or as-printed) surface was assumed to be a smooth surface, in order to provide a base line analysis in which there are no surface texture effects. The shear stress decreased from the overlap edges to the interior for the adhesive joint with the texture free surface due to the differential strain in the adherends. In contrast, the shear stress is at high levels for the inner regions of the textures where mechanical interlocking occurs for the joints with bio-mimicked surface textures. It was observed that the surface texture removed the shear stress concentration at the overlap edges seen in the texture free sample. In this way, the shear damage tolerance of the joint was increased with the bio-mimicked surface texture. In addition, compared to the adhesive surface with lamellae-surface texture, the shear stress was at a higher level in the adhesive surface with hexagon-like surface texture because the surface texture density decreased in the middle region of the bonding zone.

The peel stress distributions of the adhesive surfaces are illustrated in Fig. 10. For the adhesive surfaces with texture free and bio-mimicked surface textures, peel stress was evident at the edges of the overlap. However, the bio-mimicked surface texture reduced the maximum peel stress. This decrease was especially evident on adhesive surfaces with lamellae-like and mixed surface textures.

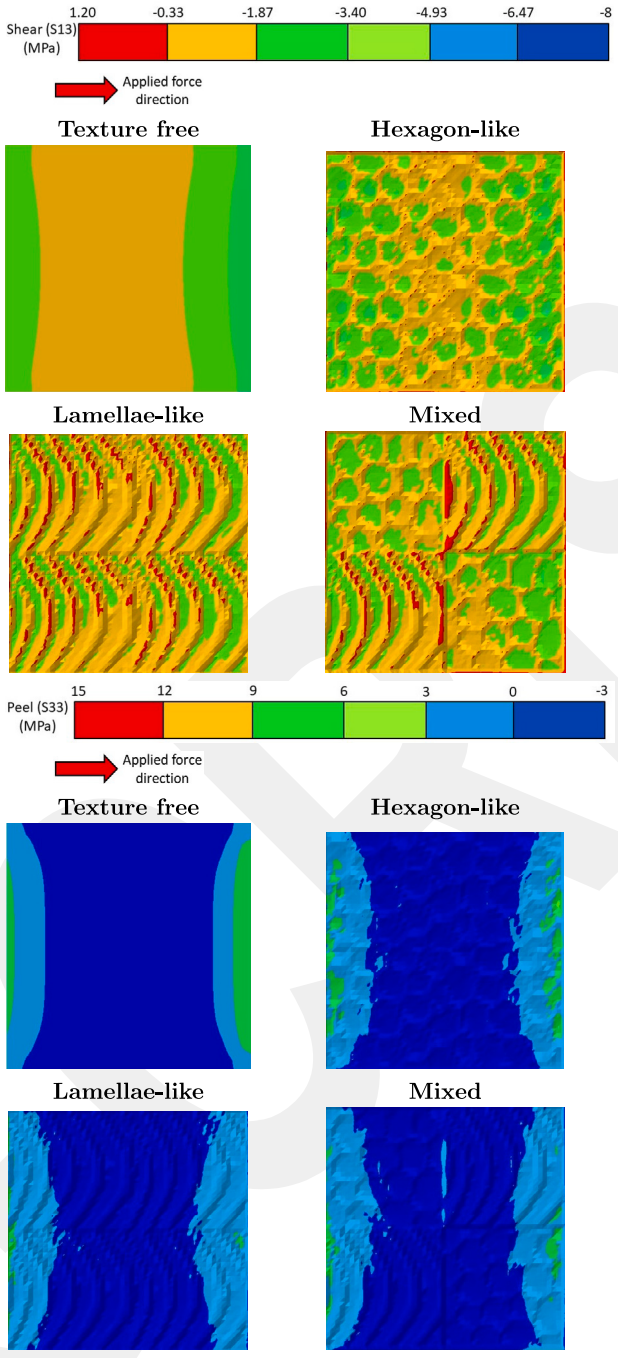

Fig. 10. Shear and peel stress distributions of the adhesive surfaces with different surface textures.

The von Mises stress distributions of the adhesive surfaces are shown in Fig. 11. A single von Mises stress index was used to compare the damage tolerance of the joints with different surface textures. The von Mises stress index varies between 0–9.5 MPa. For the joint with the texture free surface, the maximum stress occurred in the regions close to the overlap edges of the adhesive surfaces. These areas are more susceptible to damage. While the von Mises stress in the middle region of the adhesive layer was in the range of 1.58–3.16 MPa, it varied in the range of 3.16–9.5 MPa at the overlap edges of the adhesive surfaces. For the joints with bio-mimicked surface textures, the von Mises stress range decreased and local stress concentrations at the overlap edges were reduced. The von Mises stress of the adhesive layer for the joints with the bio-mimicked surface textures varied between 0–4.75 MPa. In this way, it was determined that bio-mimicked surface textures caused the joints to be damaged at higher loads, i.e, the load-carrying capacity

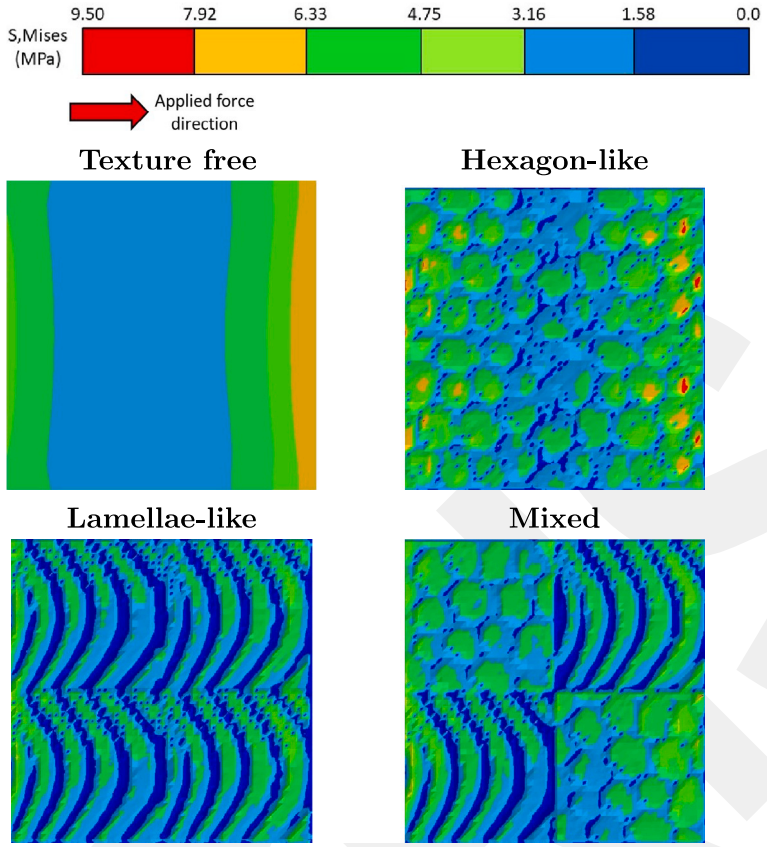

Fig. 11. von Mises stress distributions of the adhesive surfaces with different surface textures.

of the joints increased with bio-mimicked surface textures.

To summarize, it was determined that bio-mimicked surface textures reduced local shear, peel, and von Mises stress concentrations on the adhesive surface and provided a more homogeneous stress distribution. In addition, the largest stress values occurred within the surface textures, which showed that good mechanical interlocking was achieved between the adherend and the adhesive. Finally, the fact that the surface textures reduced the von Mises stress on the adhesive surfaces and provided more homogeneous stress distribution increased the damage tolerance of the joint. In this way, the strength and load-carrying capacity of the adhesive joints increased.

4.4. Failure analysis

There is a strong relationship between the adhesive damage type and the strength of the joint. Failure of adhesive joints can be categorized into four types: adhesive failure, cohesive failure, adherend failure, and mixed failure. Failure at, or close to, the adhesive–adherend interface is often called adhesive failure and is an indication that the desired mechanical interlocking between the adherends and the adhesive has not been achieved, which leads to a lower load-carrying capacity. In the cohesive failure type, the failure occurs within the adhesive layer. This failure type occurs when the interfacial strength between the adherends and the adhesive is higher than the adhesive strength. Therefore, the joint strength reaches a higher level. The cohesive failure type is the desired failure type for the adhesive joints because it increases the load-carrying capacity of adhesive joints. Adherend failure occurs when the load-carrying capacity of the joint is higher than that of the adherend. Finally, in mixed failure type, adhesive and cohesive failure types occur together in the joint [4].

Fig. 12 illustrates the fracture surfaces of adhesive joints with different surface textures. Interfacial failure (adhesive failure) was observed in joints with an as-printed surface because there was no mechanical interlocking. For this reason, the load-carrying capacity of the joint with an as-printed surface was the lowest. In the joint with the lamellae-like surface texture, the lamellar surfaces achieved mechanical interlocking and residual adhesive was visible between the lamellar patterns. However, damage mostly propagated in a region close to the interface. In the joint with the hexagon-like surface texture, the damage first initiated at the adherend–adhesive interface, then propagated through the adhesive layer, and finally passed to the other adherend–adhesive interface layer. This failure mechanism showed that good mechanical interlocking occurred between the adherend and the adhesive, and thus, it was observed that the joints with hexagon-like surface texture provided a greater increase in the load-carrying capacity

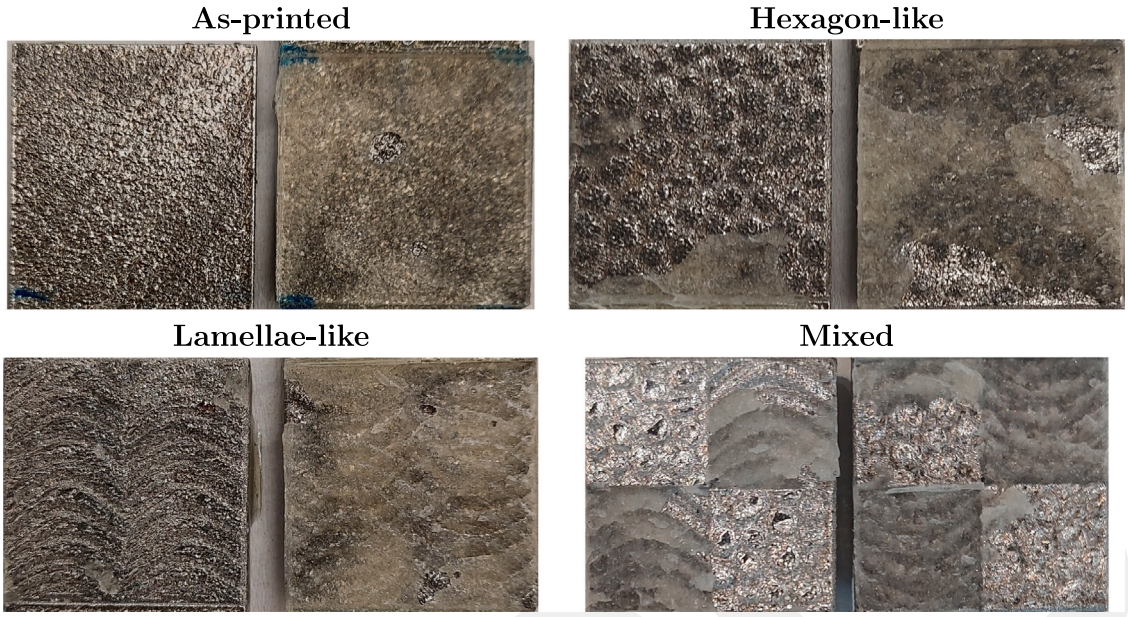

Fig. 12. Fracture surfaces of the single-lap joints.

compared to the joint with lamellae-like surface texture. A mixed failure type was observed in the joint with the mixed surface texture. Since dissimilar surface textures coincided with each other in this joint, the interfacial forces were different. This caused adhesive failure to progress both at the interfaces and within the adhesive layers, and the highest load-bearing capacity was achieved.

5. Conclusions

In this study, the effect of a bio-mimicked surface texture on the mechanical behaviour of an adhesive joint was examined experimentally and numerically. This paper presents a novel method to create bio-mimicked surface textures on bonding surfaces. The LPBF additive manufacturing method was utilized to manufacture the adherends with bio-mimicked surface textures. ASTM D1002-10 test standard was used to compare the effect of bio-mimicked surface texture on the shear strength of adhesive joints. Three different surface textures were considered based on a gecko's foot texture, toe surface texture, and a mix of them. The main results are as follows:

- Surface textures were created with the Solidworks 3D Texture command and metal adherends with bio-mimicked surface textures were successfully manufactured with the LPBF additive manufacturing method.
- Compared to the as-printed surfaces, bio-mimicked surfaces exhibited super-hydrophilic characteristics. Namely, using the bio-mimicked surface texture significantly improved wetting behaviour.
- Bio-mimicked surface textures provided a considerable increase in the lap shear strength of adhesive joints. While the highest increase in shear strength was seen in the joint with mixed surface texture due to both hexagon-like and lamellae-like surface textures being effective together in carrying shear load, the least increase occurred in the joint with lamellae-like surface texture. Hexagon-like surface texture supplied better mechanical interlocking than the lamellae-like surface texture.
- The bio-mimicked surface texture improved the damage tolerance capability of the adhesive joints by reducing local shear, peel, and von Mises stress concentrations at the overlap edges of the adhesive layer.
- While adhesive (interfacial) failure mode was observed in the joint with as-printed surface texture, mixed failure mode (cohesive and adhesive) occurred in the joints with bio-mimicked surface texture due to the mechanical interlocking effect, and this failure mode showed that the load-carrying capacity of the joint increased with using the bio-mimicked surface texture.

CRediT authorship contribution statement

M. Gokhan Atahan: Writing – review & editing, Writing – original draft, Visualization, Software, Methodology, Investigation, Conceptualization. **Ian Maskery:** Writing – review & editing, Supervision, Resources, Formal analysis, Conceptualization. **Ian Ashcroft:** Writing – review & editing, Supervision, Resources, Formal analysis. **M. Kemal Apalak:** Visualization, Software, Conceptualization. **Athanasios Pappas:** Writing – review & editing, Visualization.

Declaration of competing interest

The authors declare that they have no known competing financial interests or personal relationships that could have appeared to influence the work reported in this paper.

Acknowledgements

This research was supported by the Scientific and Technological Research Council of Türkiye (TÜBİTAK 2219-International Postdoctoral Research Fellowship Program for Turkish Citizens) and the University of Nottingham, United Kingdom. The authors extend their thanks to the U.S. National Science Foundation for usage permission of the Gecko's foot photo.

Data availability

Data will be made available on request.

References

[1] M.G. Atahan, M.K. Apalak, Experimental investigation of oblique impact behavior of adhesively bonded composite single-lap joints, Appl. Compos. Mater. 29 (3) (2022) 1293–1319.
[2] L.F. Da Silva, A. Öchsner, R.D. Adams, Handbook of Adhesion Technology, Springer Science & Business Media Verlag, Berlin Heidelberg, 2011, p. 1554.
[3] M.G. Atahan, M.K. Apalak, Finite element analysis of low-speed oblique impact behavior of adhesively bonded composite single-lap joints, Appl. Compos. Mater. 30 (3) (2023) 955–985.
[4] N. Naat, Y. Boutar, S. Naïmi, S. Mezlini, L.F.M. Da Silva, Effect of surface texture on the mechanical performance of bonded joints: a review, J. Adhes. 99 (2) (2023) 166–258.
[5] L. García-Guzmán, L. Távara, J. Reinoso, J. Justo, F. París, Fracture resistance of 3D printed adhesively bonded DCB composite specimens using structured interfaces: Experimental and theoretical study, Compos. Struct. 188 (2018) 173–184.
[6] A.T. Nguyen, M. Brandt, A.C. Orifici, S. Feih, Hierarchical surface features for improved bonding and fracture toughness of metal–metal and metal–composite bonded joints, Int. J. Adhes. Adhes. 66 (2016) 81–92.
[7] Y. Nusom, S. Srimanosaowapak, V. Uthaisangsuk, Effects of 3D-printing surface morphologies on interfacial bonding strength between Ti–6Al–4V and CFRTP with PMCs interlayer, Int. J. Adhes. Adhes. 121 (2023) 103313.
[8] J. Moritz, P. Götze, T. Schiefer, L. Stepien, A. Klotzbach, J. Standfuß, E. López, F. Brückner, C. Leyens, Additive manufacturing of titanium with different surface structures for adhesive bonding and thermal direct joining with fiber-reinforced polyether-ether-ketone (peek) for lightweight design applications, Metals 11 (2) (2021) 265.
[9] X.J. Jiang, D.J. Whitehouse, Technological shifts in surface metrology, CIRP Ann 61 (2) (2012) 815–836.
[10] A.A. Andarabi, K. Shelesh-Nezhad, T.N. Chakherlou, The effect of laser surface structuring patterns on the interfacial resistance of aluminum joints bonded with epoxy adhesive, Int. J. Adhes. Adhes. 114 (2022) 103101.
[11] M. Aripin, Z. Sajuri, S. Abdullah, M. Omar, W. Zamri, W. Jamil, M. Abdullah, Microscale groove effect on shear strength of epoxy-bonded dissimilar metal plate, J. Adhes. Sci. Technol. 30 (18) (2016) 2001–2012.
[12] L.F. Da Silva, N. Ferreira, V. Richter-Trummer, E. Marques, Effect of grooves on the strength of adhesively bonded joints, Int. J. Adhes. Adhes. 30 (8) (2010) 735–743.
[13] Z. Feng, H. Zhao, C. Tan, B. Zhu, F. Xia, Q. Wang, B. Chen, X. Song, Effect of laser texturing on the surface characteristics and bonding property of 30CrMnSiA steel adhesive joints, J. Manuf. Process. 47 (2019) 219–228.
[14] A. Hamilton, Y. Xu, M.E. Kartal, N. Gadegaard, D.M. Mulvihill, Enhancing strength and toughness of adhesive joints via micro-structured mechanical interlocking, Int. J. Adhes. Adhes. 105 (2021) 102775.
[15] N. Kumar, S. Kumar, S. Prakash, Underwater laser texturing for enhanced adhesive joint bonding strength of Al-Mg alloy, Proc. Inst. Mech. Eng. Part B: J. Eng. Manuf. 237 (10) (2023) 1461–1472.
[16] H. Li, Y. Zhu, X. Meng, S. Li, W. Du, X. Qin, Effect of laser generated microgrooves geometric parameters on the shear strength of CFRP-aluminium alloy adhesive joints, J. Adhes. 99 (10) (2023) 1744–1767.
[17] X. Liu, J. Wang, H. Bu, F. Wang, X. Zhan, Effect of groove configuration on mechanical properties and fracture behavior of 6061 Al alloy and CFRTP laser joint, Int. J. Adv. Manuf. Technol. 123 (5–6) (2022) 1913–1924.
[18] N. Öztoprak, G.M. Gençer, Load-bearing capacity of polyamide 6 (PA6) composite to 7075-O aerospace Al-alloy single-lap joints: influence of various laser textured patterns on hot press bonding, J. Adhes. Sci. Technol. (2023) 1–19.
[19] F. Sun, C. Pruncu, P. Penchev, J. Jiang, S. Dimov, B. Blackman, Influence of surface micropatterns on the mode I fracture toughness of adhesively bonded joints, Int. J. Adhes. Adhes. 103 (2020) 102718.
[20] Y. Xie, B. Yang, L. Lu, Z. Wan, X. Liu, Shear strength of bonded joints of carbon fiber reinforced plastic (CFRP) laminates enhanced by a two-step laser surface treatment, Compos. Struct. 232 (2020) 111559.
[21] Y. Zhao, J. Zang, X. Wan, B. Wang, Y. Cao, W. Wang, X. Chen, Failure mechanisms of hybrid metal–composite joints with different protrusion densities under a tensile load, Mech. Adv. Mater. Struct. (2023) 1–16.
[22] X. Zhan, J. Chen, C. Gu, Q. Peng, J. Chen, Y. Wei, Study on effects of pre-treatment and surface roughness on tensile-shear strength of 2060 Al–Li alloy adhesive joints, J. Adhes. 93 (8) (2017) 613–625.
[23] Z. Kang, Z. Shi, Y. Lei, Q. Xie, J. Zhang, Effect of the surface morphology on the bonding performance of metal/composite hybrid structures, Int. J. Adhes. Adhes. 111 (2021) 102944.
[24] F. Lambiase, P.B. Yanala, C. Leone, A. Paoletti, Influence of laser texturing strategy on thermomechanical joining of AA7075 aluminum alloy and PEEK, Compos. Struct. 315 (2023) 116974.
[25] N. Naat, Y. Boutar, S. Naïmi, S. Mezlini, L. da Silva, Effect of bio-inspired surface texture on the resistance of 3D-printed polycarbonate bonded joints, Proc. Inst. Mech. Eng. Part L: J. Materials: Des. Appl. (2022) 14644207221136239.
[26] N. Naat, Y. Boutar, S. Naïmi, S. Mezlini, L.F. da Silva, A.H. Bashiri, Influence of bio-inspired surface texture of additively manufactured 17-4 PH stainless steel adherends on the strength of adhesively bonded joints, Int. J. Adhes. Adhes. 126 (2023) 103478.
[27] M. Alfano, C. Morano, L. Bruno, M. Muzzupappa, L. Pagnotta, Analysis of debonding in bio-inspired interfaces obtained by additive manufacturing, Procedia Struct. Integr. 8 (2018) 604–609.

[28] H. Wan, J. Min, B.E. Carlson, J. Lin, C. Sun, Spindle-shaped surface microstructure inspired by directional water collection biosystems to enhance interfacial wetting and bonding strength, ACS Appl. Mater. Interfaces 13 (11) (2021) 13760–13770.
[29] H. Bu, X. Li, B. Li, X. Li, X. Zhan, Enhanced interfacial joining strength of laser wobble joined 6061-T6 Al alloy/CFRTP joint via interfacial bionic textures pre-construction, Compos. Part B: Eng. 261 (2023) 110787.
[30] J.-H. Groth, M. Magnini, C. Tuck, A. Clare, Stochastic design for additive manufacture of true biomimetic populations, Addit. Manuf. 55 (2022) 102739.
[31] U.S. National Science Foundation. https://www.nsf.gov/news/mmg/mmg_disp.jsp?med_id=66262.
[32] SOLIDWORKS 3D design software - dassault systemes. Available from: https://www.3ds.com/products-services/solidworks/?wockw=Solidworks.
[33] ASTM D1002-10, Standard Test Method for Apparent Shear Strength of Single-Lap-Joint Adhesively Bonded Metal Specimens by Tension Loading (Metal-to-Metal). URL https://www.astm.org/d1002-10r19.html.
[34] K. Autumn, M. Sitti, Y.A. Liang, A.M. Peattie, W.R. Hansen, S. Sponberg, T.W. Kenny, R. Fearing, J.N. Israelachvili, R.J. Full, Evidence for van der Waals adhesion in gecko setae, Proc. Natl. Acad. Sci. 99 (19) (2002) 12252–12256.
[35] Materialise Magics Software. Available from: https://www.materialise.com/en/industrial/software/magics-data-build-preparation.
[36] QuantAM build preparation software. Available from: https://www.renishaw.com/en/quantam-build-preparation-software--35455?srsltid=AfmBOor8My8G3SQyN7mPTSY3iZNcHHLDYUFZIZrNuGa-h753ayVparAV.
[37] Araldite standard epoxy adhesive, Huntsman Advanced Materials. http://www.huntsman.com.
[38] R.K. Behera, S. Parida, R. Das, Effect of using fibre reinforced epoxy adhesive on the strength of the adhesively bonded single lap joints, Compos. Part B: Eng. 248 (2023) 110358.
[39] D. Della Crociata, I. Maskery, R. Hague, M. Simonelli, On the development of twinning-induced plasticity in additively manufactured 316L stainless steel, Addit. Manuf. Lett. (2023) 100176.
[40] Digital Surf, MountainsMap. Available from: https://www.digitalsurf.com/software-solutions/profilometry/.
[41] ISO 25178-3:2012 geometrical product specifications (GPS) - Surface texture: Areal Part 3: Specification operators. URL https://www.iso.org/standard/42895.html.
[42] Kruss. Available from: https://www.kruss-scientific.com/en.
[43] Instron : Materials testing machines. Available from: https://www.instron.com/en/.
[44] ABAQUS, Analysis user's guide documentation version 6.13, Dassault Syst. SIMULIA Corp (2013).
[45] M.F. Ismail, M.A. Islam, B. Khorshidi, A. Tehrani-Bagha, M. Sadrzadeh, Surface characterization of thin-film composite membranes using contact angle technique: Review of quantification strategies and applications, Adv. Colloid Interface Sci. 299 (2022) 102524.
[46] R.N. Wenzel, Resistance of solid surfaces to wetting by water, Ind. Eng. Chem. 28 (8) (1936) 988–994.
[47] R.N. Wenzel, Surface roughness and contact angle, J. Phys. Chem. 53 (9) (1949) 1466–1467.
[48] C. Ye, C. Zhang, J. Zhao, Y. Dong, Effects of post-processing on the surface finish, porosity, residual stresses, and fatigue performance of additive manufactured metals: a review, J. Mater. Eng. Perform. 30 (2021) 6407–6425.